https://doi.org/10.5194/egusphere-2025-5219
Preprint. Discussion started: 11 November 2025

The impact of Aeolus observations on wind and rainfall predictions

Maurus Borne [1], Peter Knippertz [1], Michael Rennie [2], and Martin Weissmann [3]

[1]Institute of Meteorology and Climate Research Troposphere Research (IMKTRO), Karlsruhe Institute of Technology (KIT), Karlsruhe, Germany
[2]European Centre for Medium-Range Weather Forecasts (ECMWF), Reading, UK
[3]Institut für Meteorologie und Geophysik, Universität Wien, Wien, Austria

Correspondence: Maurus Borne (maurus.borne@kit.edu)

Abstract. Previous studies showed substantial improvements in upper-level wind and mass field forecasts from assimilating Aeolus wind observations. This study extends those analyses using the improved reprocessed Aeolus dataset (version B16) in experiments with the global ECMWF forecasting system spanning more than three years. Results show that zonal wind forecasts improve across the entire troposphere during the first forecast week, propagating gradually into the stratosphere, with average reductions in the Root Mean Square Error of about 0.5%, reaching over 1.5% in the tropical upper troposphere. These improvements lead to more accurate rainfall forecasts in some regions and seasons, as measured by the Fraction Skill Score (FSS) and the Stable Equitable Error in Probability Space (SEEPS). They are largest during the winter half-year in the extratropics, particularly in the Southern Hemisphere, and appear primarily at the grid scale. The largest FSS improvements, reaching several percent, occur for 5–10 day leads and heavy rainfall categories, while SEEPS indicates modest but consistent gains in categorical precipitation skill. These results suggest that assimilating Aeolus winds improves large-scale dynamics, such as jet streams and Rossby waves, leading to more accurate long-term predictions of cyclones and fronts, and ultimately better local wind and heavy rainfall forecasts.

1 Introduction

Accurate rainfall forecasts are essential for various socio-economic sectors, including agriculture, water management, transportation, and energy production. Reliable predictions enable better planning and decision-making, from optimizing irrigation and managing reservoirs to minimizing transport disruptions and supporting energy scheduling. Furthermore, precise precipitation forecasts are vital for mitigating the impacts of extreme events such as floods, landslides, and droughts by supporting early warning systems and risk management strategies. While most dynamical processes can be resolved in global Numerical Weather Prediction (NWP) models, phenomena such as radiation, turbulence, convection, clouds and precipitation are inherently too small in scale and must therefore be parameterized. Global NWP models such as the European Centre for Medium-Range Weather Forecasts' (ECMWF) Integrated Forecasting System (IFS) have made significant advances in recent years with respect to the accuracy of precipitation forecasts. In particular, advancements in the parameterization of cloud processes have improved the prediction of rainfall rates as well as their frequency distribution (Bechtold et al., 2014; Forbes et al., 2015). Despite these advancements, the accuracy of forecasts remains limited, in particular regarding predictions of

https://doi.org/10.5194/egusphere-2025-5219
Preprint. Discussion started: 11 November 2025

the location, timing, and intensity of convective precipitation events. This arises from the inherent complexity of their rapid evolution and the involved multi-scale interactions, which are not fully captured by current global NWP models using a grid spacing of about 10 km (Yang and Slingo, 2001; De Meutter et al., 2015; Prein et al., 2015; Feng et al., 2016; Taylor et al., 2017). Another key ingredient for improving precipitation forecasts is to better constrain model initial conditions through the assimilation of observations. In particular, the assimilation of spatio-temporal high-resolution satellite data, such as all-sky radiances within the ECMWF operational 4D-Variational Data Assimilation system (4D-Var), has demonstrated a significant positive impact on rainfall predictions (Bauer et al., 2010; Geer et al., 2010). In addition, the inclusion of GPS Radio Occultation (GPSRO) measurements further improved precipitation predictions by providing accurate vertical profiles of temperature and moisture (Bonafoni et al., 2019). Among the various types of atmospheric observations, wind measurements provide a particularly strong positive impact on forecast as consistently shown in several impact studies (Marseille and Stoffelen, 2003; Stoffelen et al., 2005, 2006; Žagar et al., 2008; Baker et al., 2014; Weissmann and Cardinali, 2007; Weissmann et al., 2012; Žagar, 2004). However, observations of wind are still sparse compared to satellite radiance observations that mainly constrain the mass field (Baker et al., 2014).

In response to these limitations, the European Space Agency (ESA) launched the Aeolus satellite in 2018. Aeolus was the first spaceborne Doppler wind lidar that provided direct, vertically resolved profiles of line-of sight wind across the globe (Stoffelen et al., 2005; Reitebuch, 2012; Straume et al., 2020). Operating until 2023, Aeolus filled a crucial observational gap by supplying high-accuracy wind data at altitudes important for atmospheric dynamics, such as the Upper Troposphere and Lower Stratosphere (UTLS). While previous studies have demonstrated the positive impact of Aeolus wind data on upper-air wind and mass fields (Rennie et al., 2021, 2022; Borne et al., 2023; Martin et al., 2023a; Chou and Kushner, 2024; Žagar et al., 2025), the implications for precipitation forecasting remain largely unexplored. Horizontal Wind fields are dynamically linked to precipitation processes, particularly through their influence on vertical motion, storm track evolution, and moisture transport. In the mid-latitudes, precipitation is strongly associated with the evolution of baroclinic systems (Dong et al., 2013; Ma and Chang, 2017). These are governed by upper-tropospheric jet stream dynamics and large-scale potential vorticity structures, which are highly sensitive to initial wind conditions. In the Southern Hemisphere (SH), the observational network is particularly sparse over the ocean, where midlatitude storms play a crucial role in modulating the global energy and moisture budgets. These cyclones are the primary drivers of extreme weather events during the cold season, including high winds, heavy precipitation, and abrupt temperature changes (Campbell and Renwick, 2023). In the tropics, precipitation is primarily driven by moist convection and modulated by large-scale circulation features such as Equatorial Waves (EWs) and the Madden–Julian Oscillation (MJO) (Matsuno, 1966; Wheeler and Kiladis, 1999).

The goal of this study is to assess the impact of assimilating Aeolus wind profile observations on precipitation forecasts within the ECMWF IFS. Using Observing System Experiments (OSEs) spanning more than three years (about 2/3 of the operational lifetime of the Aeolus satellite), we investigate the mean impact as well as the regional and seasonal variability of Aeolus' influence on zonal wind forecasts and its relationship to rainfall forecasts. This analysis aims to support the planning of future Aeolus follow-on DWL missions for NWP. This paper is organized as follows. We first describe the OSEs and the datasets used to validate rainfall and wind. Next, we outline the verification metrics applied to assess the impact of Aeolus on

https://doi.org/10.5194/egusphere-2025-5219
Preprint. Discussion started: 11 November 2025

both variables. The results are then presented in two parts: the first addresses the impact of Aeolus on zonal wind predictions, and the second examines the downstream effects on precipitation forecasts.

2 Data and methods

2.1 Data

In this section, we describe the experiments as well as the precipitation and reanalysis data used for verification in this study. The forecast data for both wind and precipitation are derived from two recent OSEs conducted at ECMWF, which were run with and without the assimilation of Aeolus observations. For wind, we use the ERA5 reanalysis for verification, while for precipitation, we utilize the Global Precipitation Measurement (GPM) of the Integrated Multi-satellitE Retrievals for GPM (IMERG) product.

Aeolus Observing System Experiments

Precipitation and wind forecast data were obtained from two OSEs, a widely used method in NWP to evaluate the impact of specific observation types (Bouttier and Kelly, 2001; Kelly et al., 2004). OSEs typically involve running two assimilation experiments. One of the experiments excludes the observation group of interest that are in our case Aeolus observations. In this study, two OSEs conducted at ECMWF were utilized, incorporating all operational observations plus wind observations from the Aeolus FM-B laser 4th reprocessing (DISC prototype L2B BUFR) using Baseline 16 (L1A/L1B v7.14.3 and L2B v3.90). The OSEs cover two periods: 28 June 2019 to 09 October 2020, and 10 October 2020 to 04 October 2022. Both experiments were conducted using the IFS cycle CY48R1, with a 4D-Var outer loop at TcO639 resolution, equivalent to a horizontal grid spacing of approximately 18 km. It should be noted that the data quality from the FM-B laser was initially very good but degraded over time, which has likely influenced the varying NWP impact of Aeolus observations across the two periods (Lux et al., 2025).

The processing algorithm of Aeolus wind observations distinguishes between two main types of retrievals based on atmospheric conditions: Rayleigh-clear observations, which measure backscatter from air molecules, and Mie-cloudy observations, which measure backscatter from particulates such as hydrometeors and aerosol particles. For Rayleigh-clear observations, the observation error is based on the estimated Level 2B (L2B) error, specifically the instrument error standard deviation provided by the L2B processor. The B16 configuration provides a more accurate estimate of instrument error by accounting for factors such as readout noise and dark current offset noise. For Mie-cloudy, standard error scaling is used, which includes a 2 m s^{-1} representativity error due to its higher resolution ($\sim$12 km) than the effective ECMWF model resolution. Quality control is performed using a first-guess check that rejects observations if the magnitude of departure is larger than the square root of the combined observation and background error variances multiplied by a tolerance factor of 3.5. To evaluate forecast performance, 12-hour accumulated precipitation as well as wind fields are analyzed for the 12 UTC and 00 UTC runs, with lead times

https://doi.org/10.5194/egusphere-2025-5219
Preprint. Discussion started: 11 November 2025

ranging from 24 to 240 hours (day 1 to day 10). The analysis spans the entire time of the OSEs from June 2019 to October 2022.

GPM IMERG precipitation product

For the precipitation reference product, we use the globally gridded Rainfall Integrated Multi-satellite Retrievals (IMERG) dataset (Huffman et al., 2015), which is derived from the GPM satellite constellation and other data sources and processed using the IMERG precipitation algorithm. The GPM mission is a continuation of the Tropical Rainfall Measuring Mission (TRMM), with the IMERG algorithm applied alongside additional data, including monthly surface precipitation gauge analyses, to produce a high-resolution global precipitation record. GPM IMERG is preferred over reanalysis products such as ERA5 because it relies predominantly on direct satellite observations, whereas ERA5 represents a synthesis of model output and observational data. The incorporation of model physics in such reanalyses can introduce systematic biases, particularly in regions characterized by complex topography or sparse observational coverage, thereby reducing the reliability of pointwise precipitation estimates. Nevertheless, GPM IMERG is not without limitations. Its precision decreases in regions with complex topography, such as mountain areas, where it often misinterprets cold surfaces as precipitation, leading to significant errors (Hirpa et al., 2010; Hobouchian et al., 2017). Moreover, heavy precipitation is often underestimated in warm orographic clouds (Dinku et al., 2010; Derin and Yilmaz, 2014). IMERG data can be unreliable in areas with few ground observations, complicating validation efforts (Hirpa et al., 2010). Nevertheless, the satellite product generally provides more accurate estimates in tropical wet and dry zones than in mountainous and semi-arid regions (Thiemig et al., 2012; Prakash et al., 2016; Derin et al., 2019). This dataset is gridded to a spatial resolution of $0.1° \times 0.1°$ and a temporal resolution of 30 minutes, providing near-global coverage from 60°N to 60°S. For this study, we use the "Late" (IMERG-L) product run, which is calibrated monthly with ca. 7000 ground-based meteorological stations worldwide. The precipitation data have been aggregated to match the resolution of ECMWF forecasts, i.e. a 12-hour temporal resolution on a 0.25° horizontal grid, covering the period 2000 to 2022, which provides a sufficiently long dataset suitable for building a reference climatology.

ERA5 wind reanalysis

Reanalysis datasets are widely used to evaluate changes in observing systems and to provide an independent and robust reference. Here we evaluate wind forecast accuracy using the ERA5 reanalysis dataset produced by ECMWF, as Aeolus data were not assimilated into this dataset (Hersbach et al., 2020). ERA5 is produced with an older version of the IFS 4D-Var system, CY41R2, at a horizontal resolution of 31 km.

2.2 Methods

2.2.1 Verification metrics

In this section, we outline the metrics employed to evaluate the impact of Aeolus on precipitation and wind forecasts within the ECMWF IFS. Specifically, we use the Fractions Score (FSS), the Stable Equitable Error in Probability Space (SEEPS), and

https://doi.org/10.5194/egusphere-2025-5219
Preprint. Discussion started: 11 November 2025

the Root Mean Square Error (RMSE) as detailed below. The relative improvement is calculated differently for each verification metric. For RMSE and SEEPS, which are negatively oriented, the relative improvement is computed as $\frac{(\text{Ctrl}–\text{Exp})}{\text{Ctrl}} \times 100$. For FSS, a positively oriented metric, it is calculated as $\frac{(\text{Exp}–\text{Ctrl})}{\text{Ctrl}} \times 100$. This way, positive values correspond to forecast improvement for all three metrics. Throughout the paper, regional domains are defined as follows: Northern Hemisphere (NH) from 20°N to 60°N, Tropics from 20°S to 20°N, and Southern Hemisphere (SH) from 60°S to 20°S. These boundaries are chosen to align with the latitudinal coverage of GPM IMERG precipitation data (60°S to 60°N). Beyond 60° latitude, IMERG coverage exists but with reduced accuracy, especially for extreme rainfall due to limited ground validation.

Fractions Skill Score (FSS)

The Fractions Skill Score (FSS) is a widely used spatial verification metric designed to evaluate the quality of both deterministic and probabilistic forecasts, particularly for binary events such as precipitation exceedance. The FSS compares the fraction of grid points within a specified neighborhood that exceed a given threshold in both the forecast and observations (Roberts, 2008). By calculating the squared differences between these fractions over increasing neighborhood sizes, the FSS effectively quantifies displacement errors without automatically penalizing minor location discrepancies. This approach mitigates the "double penalty" problem, where forecasts with sharp gradients are unfairly penalized if structures are slightly misplaced in space or time (Ebert, 2008).

A perfect forecast will have an FSS of 1, while a forecast with no skill will have a score of 0. Values above 0.5 are usually considered to be useful. However, the FSS becomes undefined if neither the prediction nor the observed field exceeds the threshold, unless a threshold of zero is used, in which case the score would be 1. The FSS evolves as a function of neighborhood size, providing insight into the spatial scales at which forecasts and observations are in agreement, and indicating the spatial scale at which the forecast achieves sufficient quality (Gilleland et al., 2009). Overall, the FSS provides a robust means of assessing spatial forecast accuracy, while allowing flexibility in accounting for small-scale location and intensity errors.

Stable Equitable Error in Probability Space (SEEPS)

The SEEPS score (Rodwell et al., 2010) is designed to evaluate the performance of deterministic precipitation forecasts.

The SEEPS score employs variable thresholds to classify precipitation into three categories: ‘dry,’ ‘light precipitation,’ and ‘heavy precipitation,’ based on a climatological cumulative distribution of precipitation. For this purpose, a global 20-year extended probabilistic climatology (Walz et al., 2021) from GPM IMERG observations is utilized, which aggregates all observations from previous years on a given day of the year, to have a sufficiently large window to assess rainfall probability during that day of a year. To account for interannual variability, precipitation data within a $\pm$15-day window around the target date are aggregated to estimate the day-of-year rainfall distribution. The ‘dry’ category, in accordance with World Meteorological Organization guidelines, is defined as all cases with precipitation strictly less than 0.2 mm/day. The upper limit to the ‘dry’ probability is set to 0.85 (very dry regions) in order to reduce sampling uncertainty in area-mean scores (Rodwell et al., 2010). This reduces the effective observation availability, especially in the sub-tropics.

https://doi.org/10.5194/egusphere-2025-5219
Preprint. Discussion started: 11 November 2025

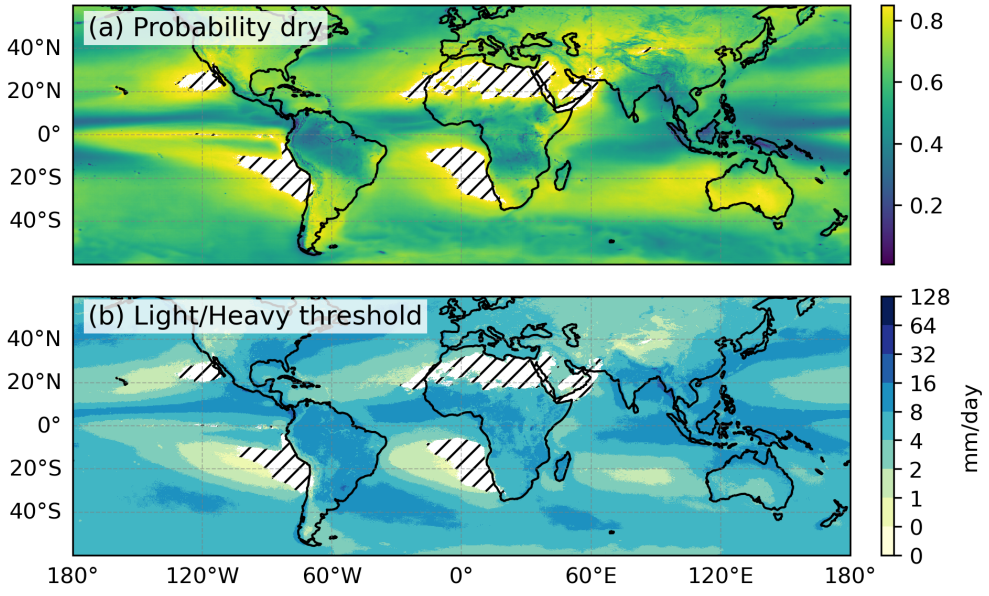

Figure 1. Geographical distribution of (a) the annual mean probability of dry conditions with respect to a day and (b) the threshold separating light and heavy precipitation categories, based on the extended GPM IMERG climatology (2000-2022). Regions where the annual probability of being dry exceeds 0.85 are indicated by hatched white areas in both panels.

.

Figure 1a displays the annual mean probability of dry days, defined as days with precipitation below 0.2 mm/day, while Figure 1b shows the annually averaged thresholds separating the light and heavy precipitation categories. These thresholds reflect local precipitation climatology, distinguishing arid from humid regions. Regions with a probability of dry days exceeding 0.85 are excluded from the analysis and are shown as hatched white areas in both panels. These masked areas typically correspond to persistently dry zones, particularly in parts of the subtropics and outer tropics, where rare precipitation events reduce the reliability of categorical verification. The light and heavy precipitation categories are defined based on local percentiles such that light precipitation occurs twice as frequently as heavy precipitation, allowing regionally consistent verification despite climatological differences.

The SEEPS score thus serves as a diagnostic to identify model errors and, as its name suggests, is constructed to ensure equitability (Murphy and Winkler, 1987; Gandin and Murphy, 1992), i.e. both constant and random forecasts receive a comparable score. In addition, SEEPS is designed to be stable, minimizing sensitivity to sampling uncertainty and allowing more accurate trends to be extracted from noisy data. Furthermore, the score operates in probability space, allowing precipitation categories to be defined in a way that adapts to the local climate, ensuring its applicability across different climatic regions.

Following Gandin and Murphy (1992), the SEEPS score is calculated as the scalar product of the scoring matrix and the 3×3 contingency table of category pairs. The scoring matrix is defined as:

https://doi.org/10.5194/egusphere-2025-5219
Preprint. Discussion started: 11 November 2025

$$S_{f,o} = \begin{bmatrix} 0 & \frac{1}{1-p_1} & \frac{1}{p_3} + \frac{1}{1-p_1} \\ \frac{1}{p_1} & 0 & \frac{1}{p_3} \\ \frac{1}{p_1} + \frac{1}{1-p_3} & 0 & 0 \end{bmatrix} \quad (1)$$

In this matrix, the rows f and columns o correspond to the forecast and observed categories, respectively: 'dry', 'light precipitation' and 'heavy precipitation'. The structure of SEEPS allows for the extraction of individual score components, providing insights into the contribution of each observed-forecast category to the overall score. In this paper, the following abbreviations are used to represent the different components of the SEEPS score: observed dry/forecast light (ODFL), observed dry/forecast heavy (ODFH), observed light/forecast dry (OLFD), observed light/forecast heavy (OLFH), observed heavy/forecast dry (OHFD), and observed heavy/forecast light (OHFL). Matching categories are represented as observed dry/forecast dry (ODFD), observed light/forecast light (OLFL), and observed heavy/forecast heavy (OHFH). Finally, note that SEEPS is a negatively oriented score, ranging from 0 to 1, where 0 represents a perfect forecast.

Root Mean Square Error (RMSE)

To evaluate the impact of Aeolus on both precipitation and wind forecasts, we also compute the traditional Root Mean Square Error (RMSE), comparing forecasts and observations at each individual location. In both OSEs, wind forecasts are verified against the ERA5 reanalysis, while precipitation forecasts are verified against GPM IMERG data. While RMSE is well-suited for normally distributed variables like wind, it is less suitable for precipitation forecasts, particularly when heavy rainfall is predicted in the wrong location. In such cases, forecasts with sharp gradients are penalized twice, once for incorrect location and again for the intensity of the event. To mitigate this "double penalty" effect, the RMSE for precipitation is computed after regridding to a coarser 1° resolution, reducing the sensitivity to slight spatial displacements of predicted rainfall events.

Significance

To evaluate the significance of forecast improvements, we apply a paired t-test at each grid point. For RMSE, the test compares the squared errors of the control and experimental forecasts relative to the reference dataset (ERA5 for wind and GPM IMERG for precipitation). For SEEPS, the test assesses the difference in SEEPS between the two forecasts. The null hypothesis is that the mean error is equal between the control and experimental forecasts. A significance level of 0.05 is used to identify statistically significant differences.

3 Results

In the first part of this section, we assess the impact of Aeolus assimilation on zonal wind forecasts, with emphasis on seasonal variations and different precipitation regimes. In the second part, we analyze the impact on precipitation forecasts using categorical and spatial verification metrics.

https://doi.org/10.5194/egusphere-2025-5219
Preprint. Discussion started: 11 November 2025

3.1 Standard verification of zonal wind forecasts

Impact of Aeolus on zonal wind forecasts

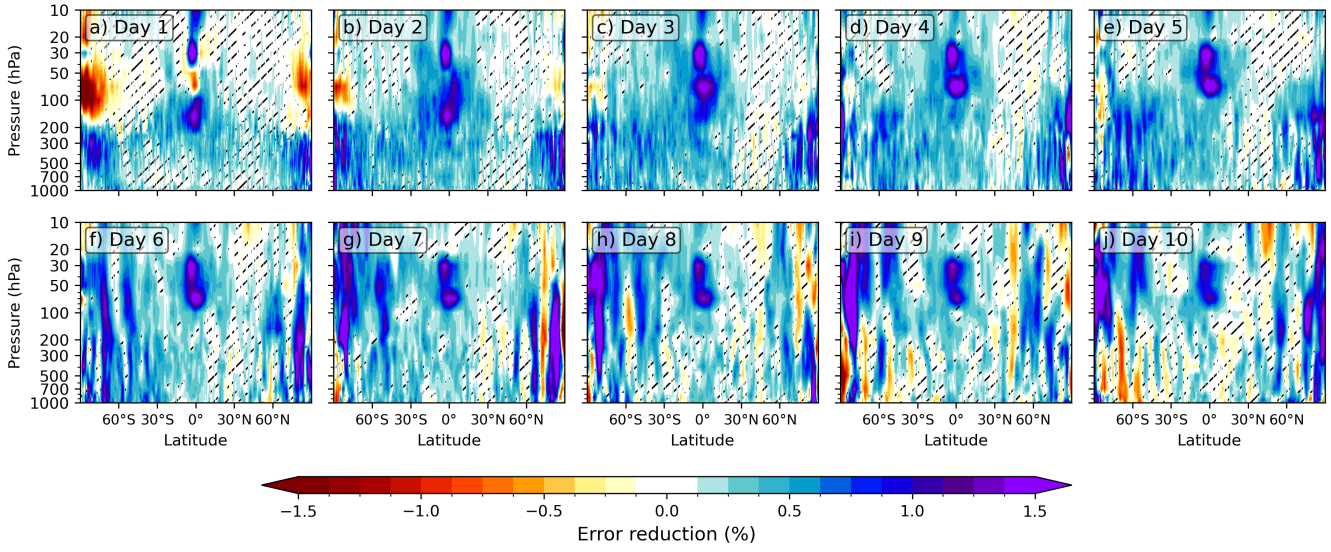

Figure 2. Zonally averaged error reduction in RMSE of zonal wind forecasts vs. ERA5 from day 1 to 10 when assimilating Aeolus wind observations, during the period 2019–2022. Positive impact is indicated in blue, while degradation is shown in red. Hatched areas denote regions where changes are not statistically significant.

.

Figure 2 shows a latitude–height cross-section of the relative improvement in the RMSE of zonal wind forecasts for lead times from day 1 to 10, when assimilating Aeolus HLOS wind observations. Hatched regions indicate areas where the improvement is not statistically significant. Results for day one in the stratosphere should be treated with caution, given uncertainty in the verification data set that may be larger than the difference between the experiments. The most pronounced impacts are observed near the equator and at high latitudes, consistent with preceding studies (Rennie and Isaksen, 2024; Rennie et al., 2021). At the equator, the largest forecast improvements occur at 20-200 hPa in the first two days and 20-100 hPa at longer lead times. The lower maximum corresponds to the upper-Tropospheric Easterly Jet (TEJ) during boreal summer, although the TEJ is not present year-round and is confined to certain longitudes (Borne et al., 2023). The upper-level maximum lies in the stratosphere and may be linked to phases of the Quasi-Biennial Oscillation (QBO) present during the experiment period, even though both easterly and westerly phases occurred. The signal could also reflect other stratospheric variability, as noted in previous studies reporting large improvements during QBO-related events (Martin et al., 2023b; Žagar et al., 2025). Notable improvements are also evident in the SH troposphere, reaching approximately 1%, along with consistent positive impact north of 60°N in the polar region. In contrast, the NH midlatitude region between 30°N and 60°N only reveals small, mostly

https://doi.org/10.5194/egusphere-2025-5219
Preprint. Discussion started: 11 November 2025

not significant, impact. The improvements in the tropics and SH are likely due to the limited coverage of conventional wind observations, such as radiosondes, and the inability of mass-field information to constrain the wind with a weaker geostrophic balance in the tropics. In high latitudes, the impact of Aeolus is may be more pronounced due to the reduced reliability of cloud-motion vectors from geostationary satellites, as the viewing geometry becomes increasingly oblique and less effective for wind retrievals. In the NH, the synoptic-scale flow is more stable, slower-evolving, and better constrained by other observations from radiosondes and aircraft. This reduces the model's sensitivity to new observations like those from Aeolus. Overall, the forecast improvements remain robust through day 7, with a gradual upward propagation into the stratosphere. From day 8 onward, the tropospheric impact is more mixed with some smaller areas of degradation.

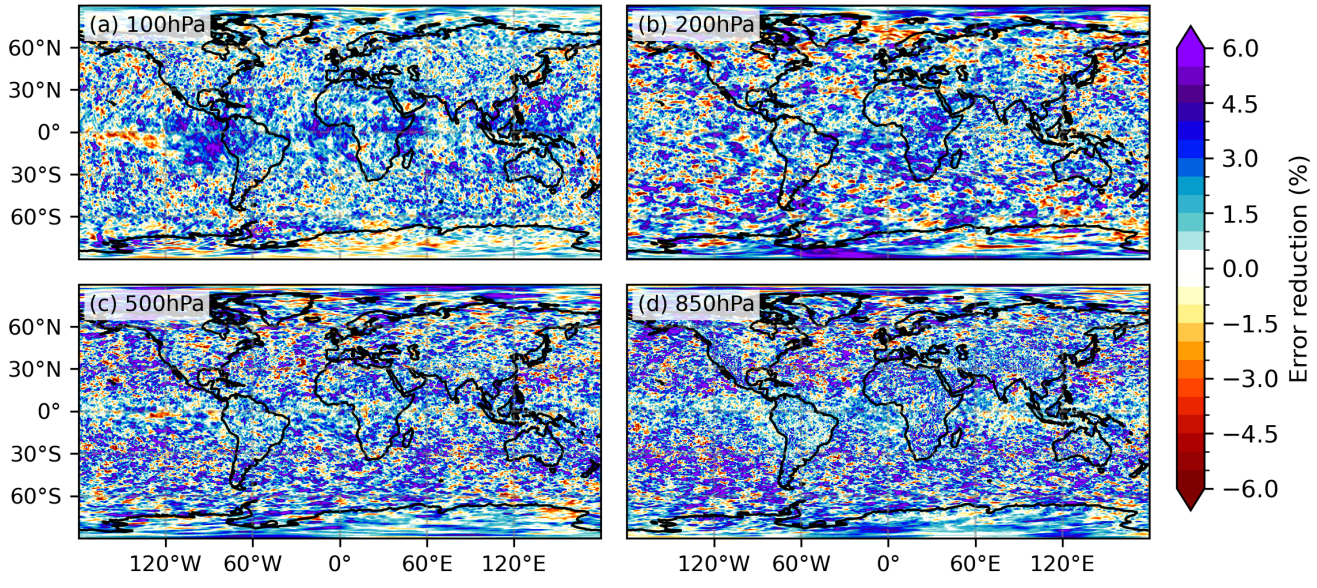

Figure 3. Error reduction in RMSE of zonal wind forecasts when assimilating Aeolus compared to ERA5 at a 3-day forecast range for pressure levels of (a) 100 hPa, (b) 200 hPa, (c) 500 hPa and (d) 850 hPa.

.

Figure 3 illustrates the impact of Aeolus assimilation on 3-day wind forecasts at pressure levels of 100, 200, 500, and 850 hPa. Overall, mean improvements are observed globally across all levels. At 100 hPa, the most pronounced improvements occur in the eastern Pacific near Central America, the western Pacific near the Maritime Continent, and a patchy region stretching from the western Indian Ocean across East Africa into the tropical eastern Atlantic, associated with the TEJ during boreal summer (see Borne et al. (2023)). At 200 hPa (Fig. 3b), the impact of Aeolus assimilation is more spatially heterogeneous, with significant positive improvements exceeding 4%, particularly over Africa and the tropical Atlantic. Similar positive patterns, but with an increasing level of noisiness, are observed at 500 hPa (Fig. 3c) and 850 hPa (Fig. 3d), with the strongest effects in extratropical regions. The smaller impact in the tropical lower troposphere is attributed to Aeolus' limited ability to sample winds beneath convective cloud cover.

https://doi.org/10.5194/egusphere-2025-5219
Preprint. Discussion started: 11 November 2025

Seasonal Dependence on Wind Forecast

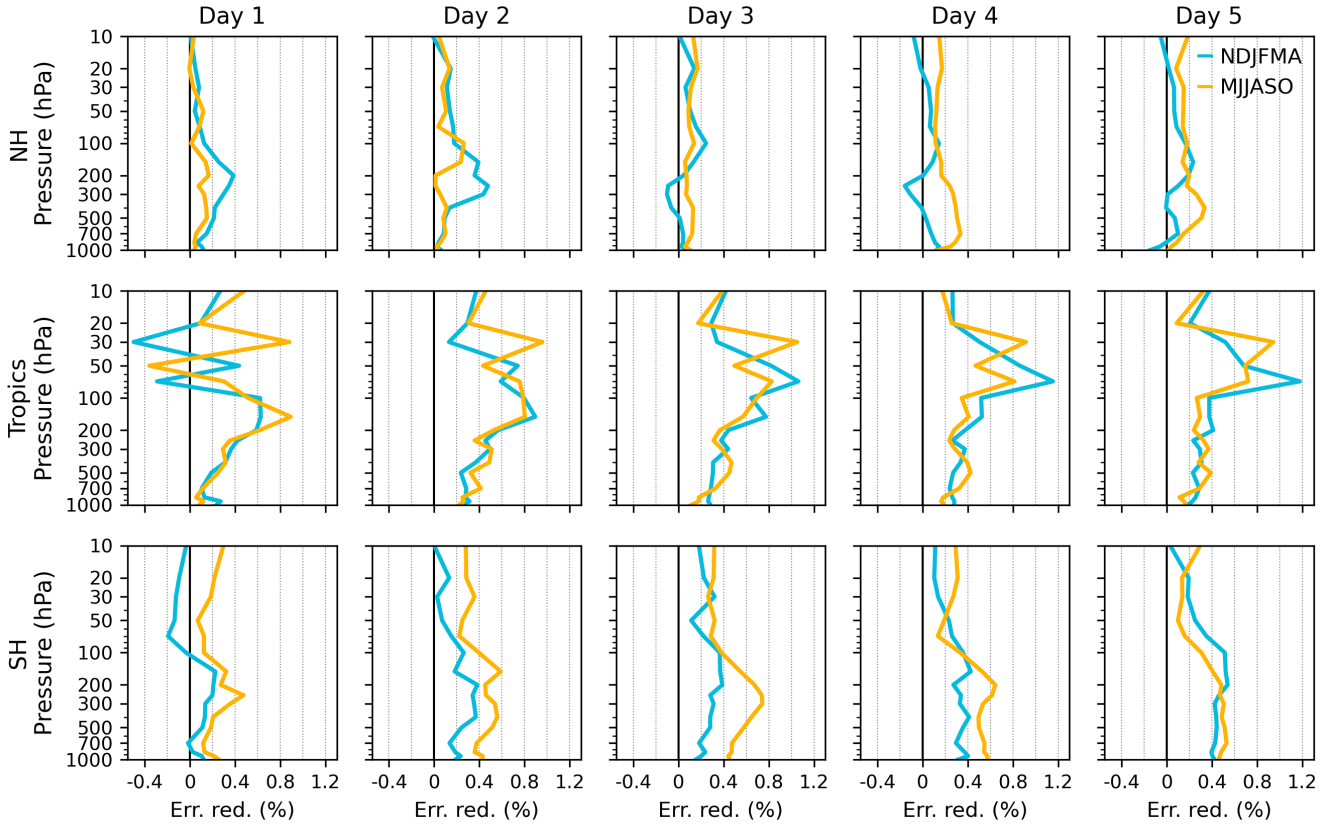

Figure 4. Reduction of RMSE in zonal wind forecasts through the assimilation of Aeolus observations relative to ERA5, averaged over the Northern Hemisphere (20°N–60°N), Tropics (20°S–20°N), and Southern Hemisphere (60°S–20°S), for forecast days 1 to 5. Results are stratified by extended season: NDJFMA (extended boreal winter, blue) and MJJASO (extended austral winter, orange)

.

To examine the seasonal behavior of zonal wind forecast improvement, Fig. 4 shows the relative RMSE reduction from Aeolus wind observation assimilation for the extended boreal winter (NDJFMA, blue line) and the extended austral winter (MJJASO, orange line) during the first five forecast days, stratified by hemisphere (NH, Tropics, and SH).

In the NH (top row), during the extended boreal winter, a notably stronger improvement is observed in the upper troposphere (500–100 hPa) for forecast days 1 and 2, with error reductions reaching up to 0.4%, compared to 0.1–0.2% during the extended summer. Above 100 hPa, in the stratosphere, both seasons show similar performance. From day 3 onward, the improvement during boreal winter declines, particularly below 200 hPa, resulting in a near-neutral impact. In contrast, during summer, the impact is more consistent for different lead times, with an average error reduction of 0.2–0.3%.

https://doi.org/10.5194/egusphere-2025-5219
Preprint. Discussion started: 11 November 2025

In the Tropics (middle row), seasonal differences are minimal throughout the vertical profile, reflecting the weak seasonality of the tropical circulation, where inter-seasonal variability is often larger than the seasonal cycle due to phenomena such as the MJO and EWs. In contrast, in the tropical stratosphere, Aeolus assimilation exhibits clear seasonal peaks in forecast improvements, for example around 30 hPa during MJJASO and 50 hPa during NDJFMA. The seasonal difference in peak altitude could reflect the vertical shift of the tropical stratospheric eastward wind, which is typically stronger and lower (~30 hPa) in boreal summer (MJJASO) and higher (~50 hPa) in boreal winter (NDJFMA), so Aeolus observations have the largest impact where the zonal wind is strongest.

In the SH (bottom row), a clear seasonal signal is evident with consistently larger impact during the extended austral winter than during the extended austral summer. The error reduction extends from the surface to the lower stratosphere with a peak in the UTLS region. For day 3 and 4, the benefit during austral winter increases to a maximum of 0.6 - 0.8% RMSE reduction near 300 hPa, compared to 0.4% during austral summer. Above 100 hPa, the seasonal contrast is less distinct and by day 5, the contrast between seasons becomes less pronounced overall; forecast improvement remains slightly larger for austral winter below 200 hPa, while above this level, summer forecasts show larger improvement. The larger Aeolus impact in the SH during austral winter may be due to increased baroclinic activity and associated rapidly growing forecast errors. In such conditions, Aeolus wind profiles likely help to better constrain the atmosphere and thereby improve forecasts.

Wind Forecast Improvements in Different Precipitation Regimes

In this section, we investigate how the impact of Aeolus wind assimilation varies under different precipitation regimes. The underlying hypothesis is that Aeolus winds are less beneficial in regions of deep convection and thick cloud cover, where lidar signal attenuation or blockage reduces measurement quality, and where moist convective processes introduce greater forecast uncertainty. To evaluate the sensitivity of Aeolus wind assimilation to precipitation regimes, we applied a rainfall mask to categorize forecast conditions into dry, light, heavy, and all conditions without masking. While precipitation categories do not perfectly reflect cloud presence or type, since non-precipitating clouds and both convective and stratiform systems can occur, they still provide a statistical tendency to distinguish conditions more likely to involve deep, thick clouds (heavy or light precipitation) from those generally associated with clearer skies (dry conditions). This distinction is relevant because Aeolus wind quality has been shown to degrade in cloudy environments due to signal attenuation and contamination, particularly in the presence of thick cloud (Borne et al., 2024).

Figure 5 presents the relative RMSE reduction in zonal wind forecasts over the first five forecast days for each precipitation category across three regions: the NH (20°N–60°N), the tropics (20°S–20°N), and the SH (60°S–20°S). The clearest signal emerges in the tropics, where dry conditions consistently show greater forecast improvements compared to light or heavy precipitation cases. At 150 hPa on forecast day 1, RMSE reductions reach up to 1 % under dry conditions, compared to approximately 0.3–0.4 % in rainy regimes. The strongest improvements occur in persistently dry regions (Fig. 1a) and may be linked to key areas of forecast enhancement in the UTLS depicted in Figure 3. This contrast across precipitation regimes gradually decreases with lead time and becomes negligible by day 5. Additionally, we observe a vertical shift of the maximum impact into the stratosphere (above 100 hPa) at longer lead times, where differences across precipitation categories also become

https://doi.org/10.5194/egusphere-2025-5219
Preprint. Discussion started: 11 November 2025

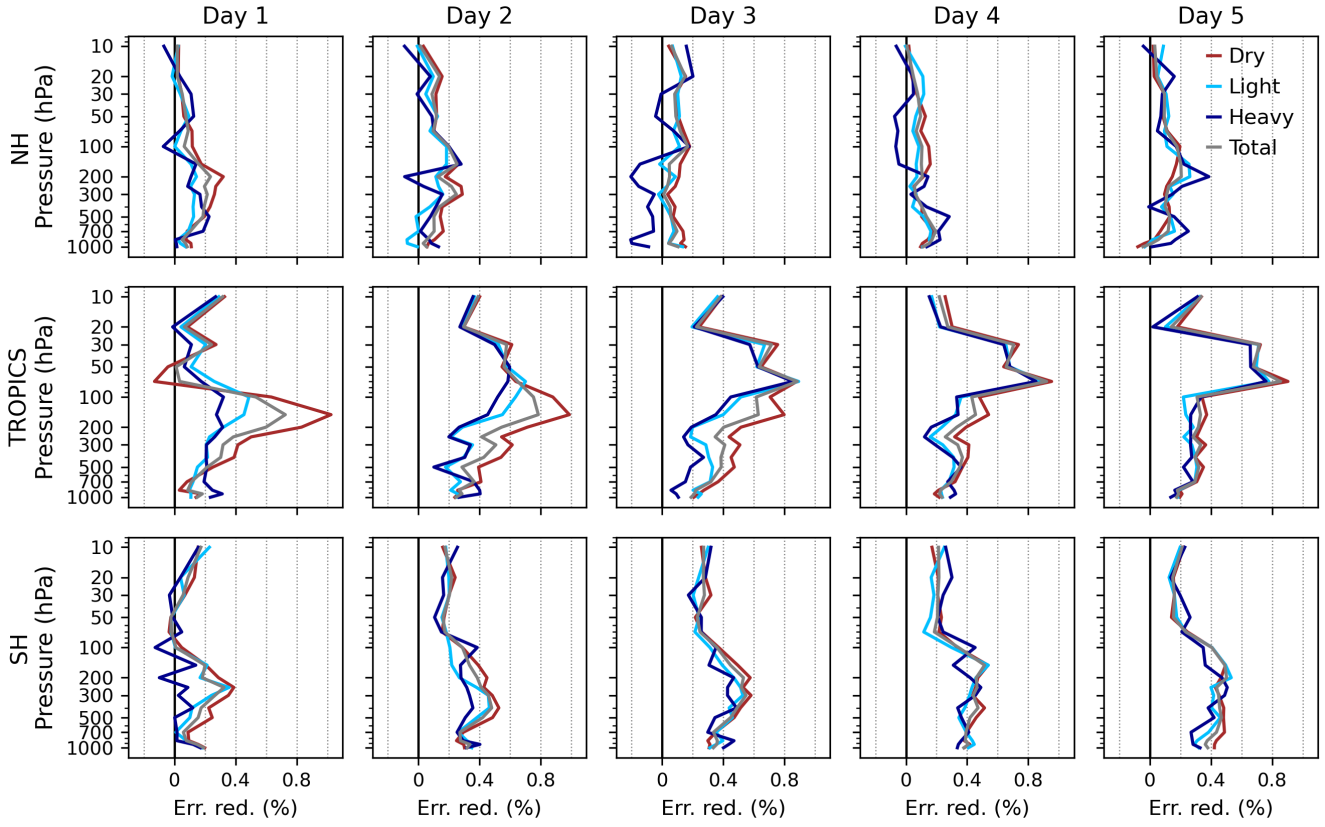

Figure 5. Reduction of RMSE in zonal wind forecasts through the assimilation of Aeolus observations relative to ERA5, averaged over the Northern Hemisphere (20°N–60°N), Tropics (20°S–20°N), and Southern Hemisphere (60°S–20°S), for forecast days 1 to 5. Results are stratified by precipitation intensity using rainfall masks: dry (brown), light (light blue), heavy (dark blue), and without a precipitation mask (grey) conditions.

.

minimal. These levels are generally above all cloud layers and therefore less affected by surface precipitation regimes. In the SH, peak improvements are observed near 300 hPa, with dry conditions showing slightly greater RMSE reductions (0.4–0.5%) compared to rainy regimes. In the SH stratosphere, however, the impact remains limited, with reductions around 0.2% across all categories. In the NH, the response is more uniform across precipitation regimes, with relatively consistent improvements of 0.1–0.2% throughout the vertical profile. This weaker signal likely reflects the denser observational network in the NH compared to the tropics and the SH.

https://doi.org/10.5194/egusphere-2025-5219
Preprint. Discussion started: 11 November 2025

3.2 Precipitation Forecast Verification

This section evaluates the impact of Aeolus wind assimilation on precipitation forecasts using FSS and SEEPS (see Section 2.2.1 for their descriptions). These metrics provide complementary insights into categorical and spatial-scale forecast performance, respectively.

Spatial-Scale Dependence: Fractions Score (FSS)

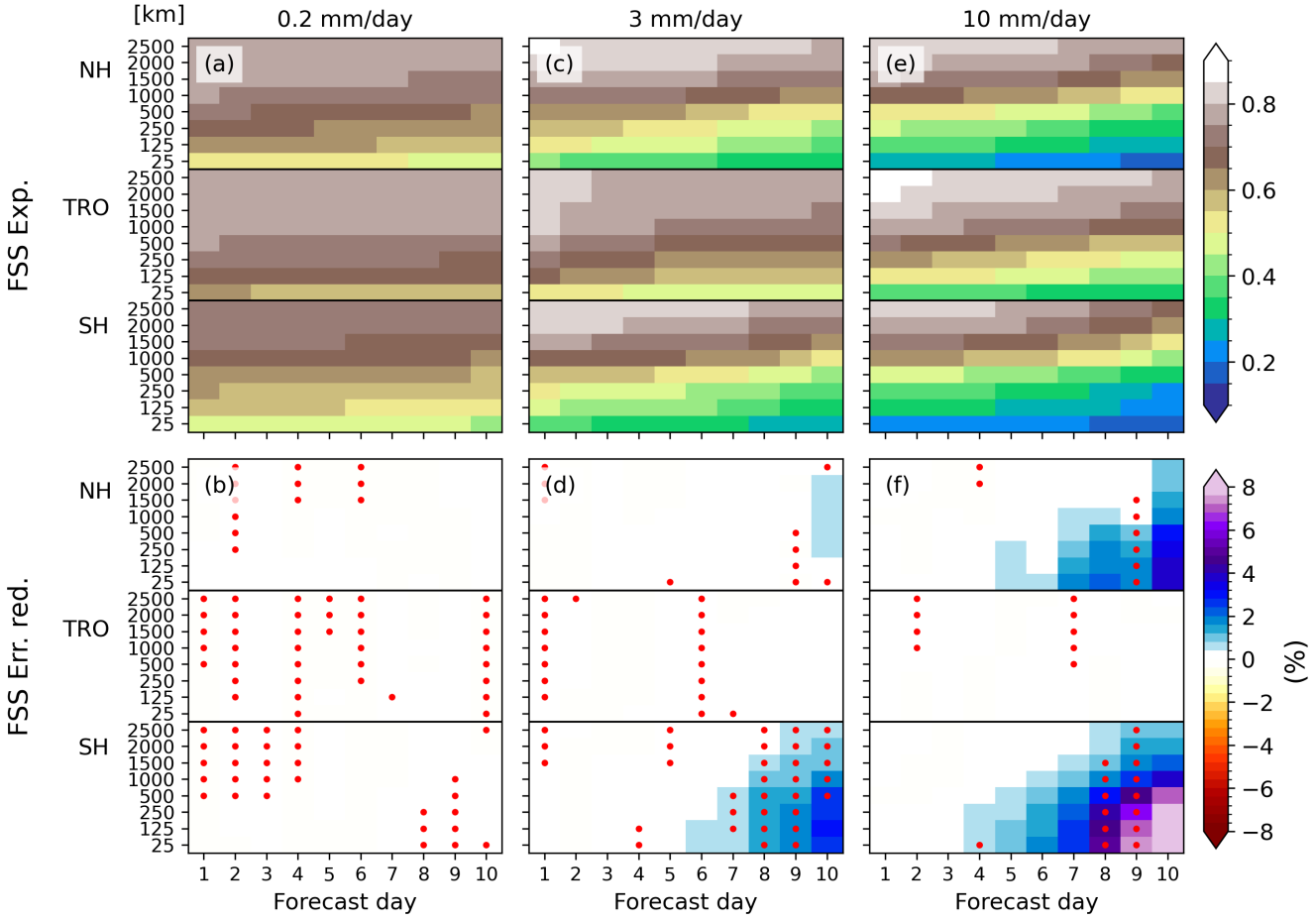

Figure 6. Top Row: Fraction Score (FSS) of the experiment assimilating Aeolus (Exp), displayed across different scales and regions (Northern Hemisphere (NH), Tropics (TRO) and Southern Hemisphere (SH)) for thresholds of 0.2 mm/day (a), 3 mm/day (c), and 10 mm/day (e). Bottom Row: Relative improvement in FSS (%) due to Aeolus assimilation, computed as the percentage difference between Exp and the control experiment (CTRL), presented in the same format. Red dots indicate statistically significant improvements at the 95% confidence level (paired t-test).

https://doi.org/10.5194/egusphere-2025-5219
Preprint. Discussion started: 11 November 2025

Figure 6 presents the FSS across spatial scales ranging from approximately 25 km to 2500 km and for three precipitation thresholds (0.2, 3, and 10 mm/day). Results are shown separately for the Northern Hemisphere (NH), Tropics, and Southern Hemisphere (SH), together with the corresponding error reduction in FSS when assimilating Aeolus wind observations.

FSS values decrease with increasing precipitation thresholds and decreasing spatial scales (Fig. 6a,c,e), reflecting the increasing difficulty of accurately forecasting heavier precipitation at finer scales. This behavior is particularly pronounced in the extratropics (Fig. 6b,d,f).

The assimilation of Aeolus winds shows a clear positive impact in both hemispheres, with the SH exhibiting the most consistent and substantial improvements, particularly at small and medium spatial scales. At higher thresholds (10 mm/day), FSS improvements emerge as early as forecast day 4 at the smallest scales (approximately 25 km), reaching more than 8 % by day 10. At lower thresholds (0.2 mm/day), no visible improvement is detected, indicating negligible impact on light precipitation. The spatial structure of the improvements indicates that gains are largest where forecast skill is low (FSS < 0.5). Moreover, the range of affected scales broadens with forecast lead time, eventually encompassing the largest scales (approximately 2500 km) by day 5. Statistically significant improvements are most evident for days 7–10 at the 3 mm/day threshold and for days 8–9 at 10 mm/day, suggesting that Aeolus contributes to a better representation of heavy rainfall events in the SH, likely due to the limited availability of in situ wind observations in this region.

In the NH, the response is qualitatively similar but weaker in magnitude. The largest improvements occur for the 10 mm/day threshold after forecast day 5, exceeding 2 % beyond day 7. In contrast, at lower thresholds (0.2 and 3 mm/day), no appreciable impact is observed, suggesting that Aeolus assimilation exerts little influence on light precipitation while providing clearer benefits for intense rainfall events.

In the Tropics, Aeolus assimilation has negligible impact across all thresholds, with error reductions close to zero and no discernible spatial or temporal pattern. Although isolated areas exhibit statistically significant signals, their magnitude remains minimal, indicating that the significance arises from small but systematic differences rather than from substantial forecast improvements.

Categorical Dependence: Stable Equitable Error in Probability Space (SEEPS)

Having assessed the impact of Aeolus assimilation on precipitation forecasts using the FSS, which revealed the largest improvements at the grid scale, we now examine a grid-scale categorical verification metric, SEEPS, to further quantify forecast skill.

Figure 7 presents the relative error reduction in SEEPS (brown line), alongside the corresponding reduction in RMSE of rainfall forecasts (red line), with RMSE values aggregated to a 1° grid to reduce the double-penalty effect commonly seen in precipitation verification. Statistical significance is indicated by dots (significant) and crosses (not significant). In addition, the colored bars identify the dominant precipitation category (dry, light, or heavy) contributing to changes in the SEEPS score at each lead time. Overall, the average impact of Aeolus assimilation on precipitation forecasts, as measured by SEEPS and RMSE over the full study period, is relatively modest. In the NH (Fig. 7a), SEEPS improvements remain close to zero across all lead times, although most values are statistically significant. The RMSE of rainfall forecasts exhibits minor fluctuations around

https://doi.org/10.5194/egusphere-2025-5219
Preprint. Discussion started: 11 November 2025

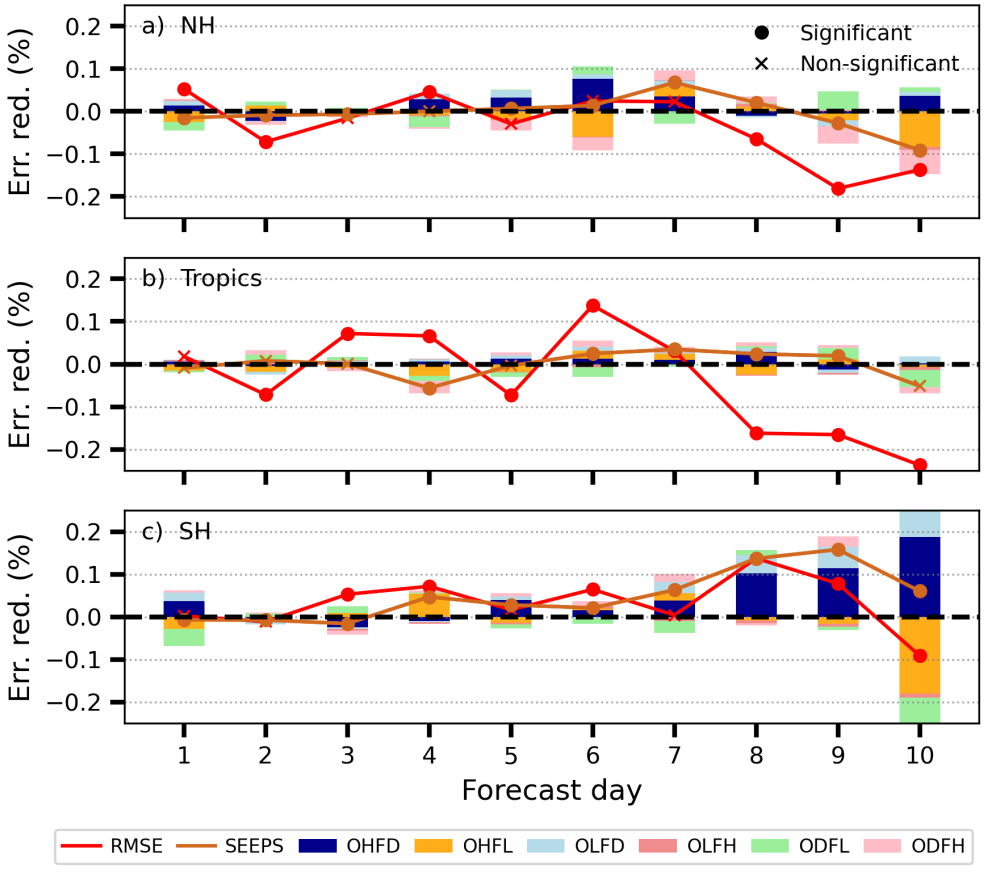

Figure 7. Relative improvement in RMSE (red line) and SEEPS score (brown line), alongside the SEEPS score subcategories (bars), when assimilating Aeolus for different regions: Northern Hemisphere (20°N-60°N) (a), Tropics (20°S-20°N) (b), and Southern Hemisphere (20°S-60°S) (c). The scores are expressed as percentages, with positive values indicating a benefit from Aeolus assimilation. Circles indicate statistically significant results, while crosses denote non-significant scores.

zero, indicating limited and inconsistent forecast improvement in this region. In the Tropics (Fig. 7b), SEEPS shows predominantly non-significant changes during the first five days. From day 6 onwards, small but statistically significant improvements emerge, reaching approximately 0.03% by day 9. However, no precipitation forecast category dominates the contribution to this improvement. The corresponding RMSE displays a similarly variable pattern with no strong trend, highlighting the challenge of achieving consistent forecast gains in convectively active regions. In contrast, the SH (Fig. 7c) demonstrates more coherent improvements. Statistically significant increases in SEEPS become evident from day 4 onward, rising steadily to about 0.15% by day 9. Notably, from days 7 to 10, the SEEPS gains are primarily driven by improvements in the OHDF (Observed Heavy, Forecast Dry) category, suggesting that Aeolus contributes to reducing false dry and light forecasts during heavy precipitation

https://doi.org/10.5194/egusphere-2025-5219
Preprint. Discussion started: 11 November 2025

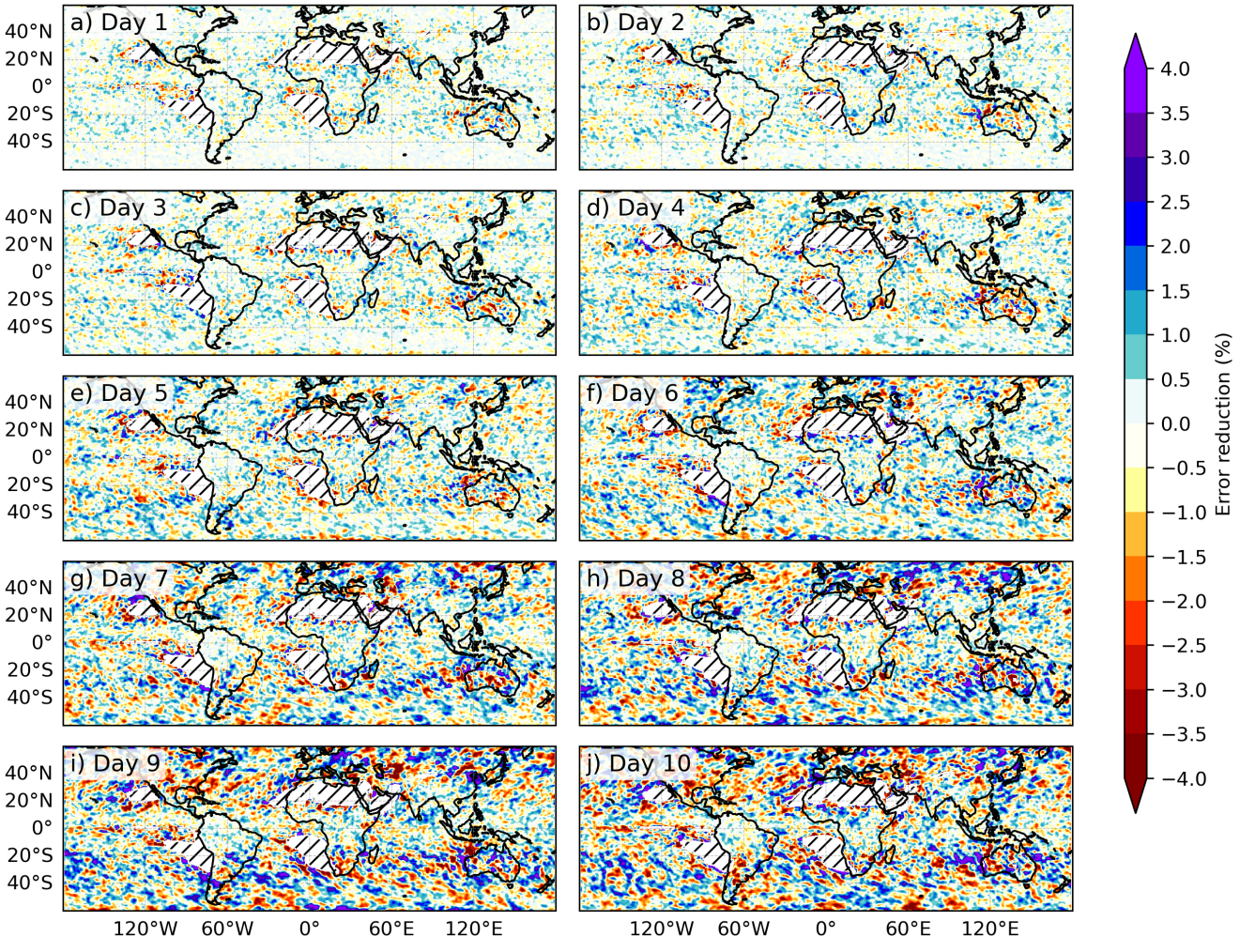

Figure 8. SEEPS error reduction for all 10 forecast lead times. A 5-grid-point rolling window has been applied to spatially smooth the signal and reduce noise. Hatched white areas denote regions where the probability of dry conditions exceeds 85% throughout the year (see Fig. 1).

events. The rainfall RMSE in the SH also shows a clear signal of consistent and significant improvements from day 3 to day 9, averaging around 0.05%.

Figure 8 presents the geographical distribution of relative changes in the SEEPS score across forecast lead times. Overall, the impact of Aeolus assimilation on precipitation forecasts is spatially heterogeneous, with no region showing consistently strong or persistent signals. However, the amplitude of relative score variations is notably larger in the Tropics compared to the NH and SH during the first three forecast days, suggesting greater forecast sensitivity in this region. While patterns of error reduction vary over time, some regions show notable early improvements. For example, at forecast days 1 and 2 (Figures 8a,b), localized enhancements in SEEPS of up to 1 % are seen over northeastern Africa, a climatologically rather dry area. These

https://doi.org/10.5194/egusphere-2025-5219
Preprint. Discussion started: 11 November 2025

early tropical signals are consistent with the dry-region patterns identified in Fig. 1 and correspond to the upper-tropospheric zonal wind improvements shown in Fig. 3a. At longer lead times, particularly after day 7, more pronounced improvements are observed in the SH, especially over the Southern Ocean.

These gains align with the positive trends seen in Fig. 7c, highlighting Aeolus's extended-range contribution to precipitation forecast in this region.

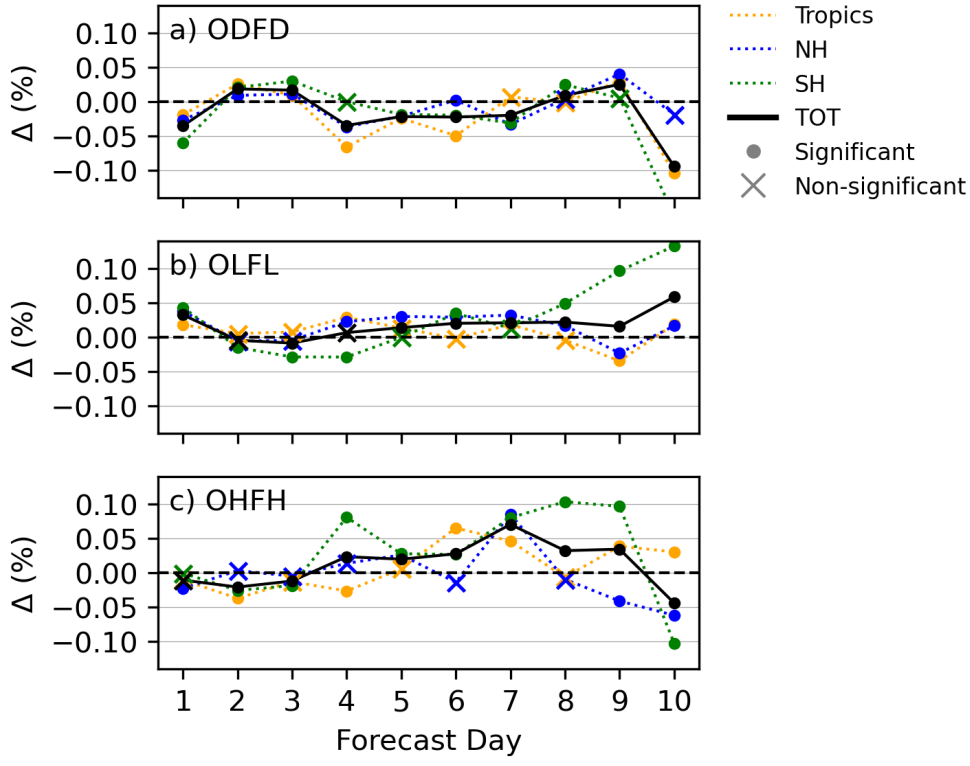

Figure 9. Change in correct rain category forecasts (%) with Aeolus wind assimilation over lead time for ODFD (a), OLFL (b), and OHFH (c), relative to total OD, OL, and OH events, respectively. Results are shown for the Tropics (orange), NH (blue), SH (green), and global (black). Circles indicate statistically significant changes ($p < 0.05$) based on a chi-squared test; crosses denote non-significant changes.

Next, we assess changes in ECMWF categorical precipitation forecasts. Figure 9 presents the relative changes in the proportion of correctly predicted precipitation categories for ODFD (a), OLFL (b), and OHFH (c), which represent correct forecasts of dry, light, and heavy precipitation, respectively. The evaluation is performed across the Tropics, Northern Hemisphere (NH), Southern Hemisphere (SH), and globally (TOT). Importantly, this analysis includes all available forecast–observation pairs, including cases where the probability of dryness exceeds 0.85 %. This ensures a more complete assessment of categorical forecast performance, beyond the subset used for SEEPS. Statistical significance of the differences is assessed using a chi-squared test, with circles indicating significant improvement and crosses indicating non-significant changes. For the ODFD

https://doi.org/10.5194/egusphere-2025-5219
Preprint. Discussion started: 11 November 2025

category (Observed Dry Forecast Dry), a small but statistically significant increase across all regions (up to 0.02%) is observed at forecast days 2 and 3, followed by a decline between days 4–7, and a modest rise again toward day 9.

The OLFL category (Observed Light Forecast Light) shows a more sustained improvement, starting around day 4 and increasing gradually to 0.05% by day 9. The enhancement is most pronounced in the NH during early leads, while the SH reveals a modest degradation for days 2-4 followed by increased improvement at longer lead times, reaching up to 0.15% by day 10. Changes in the tropics are inconsistent between lead times and often rather small. Here light rain often occurs at the edges of convective systems, e.g. in the stratiform part of big organized clusters. The lack of improvement therefore, once again, appears to reflect the difficulty to forecast tropical convection in a more general sense.

The OHFH category (Observed Heavy Forecast Heavy) displays the most substantial and statistically significant gains. An increase begins around day 4, peaking near 0.07% at day 7, then slightly tapering off by day 10. The signal is primarily driven by the SH and the Tropics, while NH improvements remain more modest. These results suggest that Aeolus assimilation improves the prediction of heavy precipitation events.

Seasonal Dependence of Precipitation Forecast Improvements

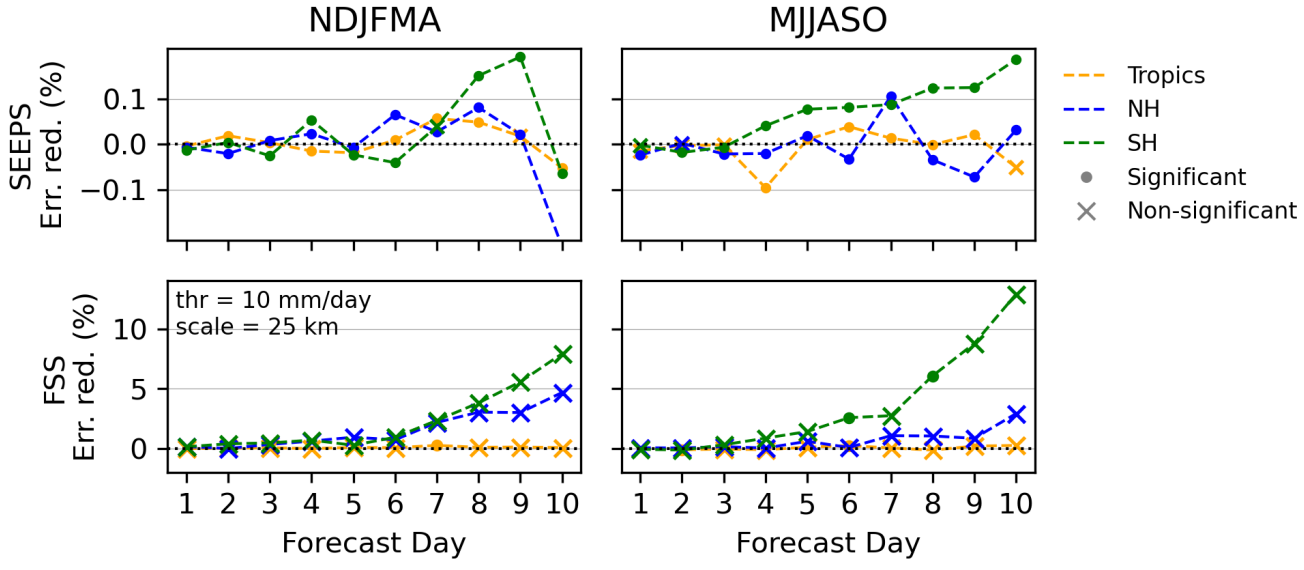

Figure 10. SEEPS (top) and FSS (bottom) error reduction for NDJFMA (left) and MJJASO (right) seasons, shown by forecast day (1–10) across three regions: Tropics, NH, and SH. Dots indicate statistically significant improvements, and crosses denote non-significant differences. FSS is computed using a 10 mm/day threshold and 25 km spatial scale.

Figure 10 presents the seasonal impact of assimilating Aeolus wind profiles on precipitation forecast error reduction, assessed using SEEPS and FSS metrics, for the extended boreal winter (NDJFMA) and summer (MJJASO) periods.

https://doi.org/10.5194/egusphere-2025-5219
Preprint. Discussion started: 11 November 2025

In the NH, forecast improvements are notably greater during the extended boreal winter season. SEEPS error reduction becomes statistically significant after forecast day 3, peaking at approximately 0.08% by day 6. Similarly, FSS shows meaningful improvements from day 5 onward, reaching around 5% error reduction by day 10. In contrast, during the extended summer season, SEEPS displays more variable error reduction, with only modest improvements. FSS shows a slight increase after day 7, rising from about 1% to 3% by day 10. This pronounced seasonal dependence likely reflects the dominance of baroclinic systems during boreal winter, which are more dynamically predictable and highly sensitive to initial condition errors in the wind field. The presence of a stronger, more coherent polar jet stream during winter enhances the value of accurate upper-tropospheric wind observations, such as those provided by Aeolus. This interpretation is supported by the marked improvement in NH zonal wind forecasts during NDJFMA (Fig. 4), suggesting that enhanced wind initializations translate into more ful precipitation forecasts under wintertime dynamics. During extended summer, weaker dynamical forcing result in lower predictability and smaller, less consistent forecast gains.

In the SH, the seasonal pattern is largely consistent with that of the NH. While some marginal improvement is observed in the extended austral summer (NDJFMA), forecast gains are notably greater during the extended austral winter (MJJASO). SEEPS improvements become detectable from day 4 ($\sim$ 0.05%) and steadily increase to 0.2% by day 10, while FSS improvements rise sharply from 1% to 15%. These gains coincide with marked improvements in SH zonal wind forecasts (Fig. 4). This enhanced performance is likely linked to the stronger SH jet stream, especially over the large ocean areas where conventional observations are limited. Aeolus thus provides a valuable source of upper-level wind data over the SH oceans, improving the representation of dynamically active regions such as mid-latitude storm tracks, and consequently leading to more skillful precipitation forecasts.

In the Tropics, improvements are generally weaker and less seasonally dependent. SEEPS shows modest gains after day 6 in both NDJFMA and MJJASO, but FSS indicates negligible error reduction. This likely reflects the inherent predictability limits of tropical convection, which is strongly influenced by mesoscale and sub-grid processes such as moist convection and diurnal heating, phenomena that are less sensitive to synoptic-scale wind information.

4 Conclusions

This study evaluates the impact of assimilating Aeolus wind profiles on both wind and precipitation forecast performance within the European Centre for Medium-Range Weather Forecasts (ECMWF) Integrated Forecasting System (IFS). Based on a three-year Observing System Experiment (OSE) using Baseline 16 of the fourth reprocessing dataset, the results highlight significant improvements in upper-tropospheric wind forecasts and demonstrate downstream benefits for precipitation forecasts in some regions and seasons.

Aeolus has its strongest influence on wind fields in the upper troposphere and lower stratosphere of the tropics, where conventional wind data are limited and mass fields provide only weak constraints. In this region, zonal wind forecast errors decrease by as much as 1% during the first week of the forecast, with particularly clear benefits over the Maritime Continent, the tropical Atlantic–African sector near the Tropical Easterly Jet, and the eastern Pacific. The strongest gains occur in cli-

https://doi.org/10.5194/egusphere-2025-5219
Preprint. Discussion started: 11 November 2025

matologically dry areas, where conventional wind data are limited, no cloud-motion vector winds exist, and reduced cloud contamination further improves measurement quality. Seasonal variations in the troposphere are small, since tropical circulation is more strongly controlled by EWs and convection than by the annual cycle. The impact on tropical rainfall is modest, with Stable Equitable Error in Probability Space (SEEPS) improvements appearing only after day 7 and remaining close to 0.03%, while Fraction Skill Score (FSS) picks up a slight but consistent signal at thresholds above 10 mm/day, reaching about 0.1%.

The largest impacts in the Southern Hemisphere (SH) occur during the extended austral winter (May to October) when the polar jet strengthens and becomes more zonal. In this season, zonal wind error declines by more than 1.5% in the troposphere and the reduction gradually propagates upward into the stratosphere by day 10. These dynamical improvements are also propagated into the precipitation forecasts. The FSS, which is highly sensitive to the spatial organization of rainfall, exhibits clear improvements, particularly at the grid scale and for heavy precipitation and long leadtimes. During the austral winter season, gains appear as early as day 3, exceed 2 % by day 8, and reach approximately 15 % by day 10. The SEEPS metric corroborates these results, showing a steady reduction in categorical errors from around 0.05 % at day 3 to 0.2 % by day 10. At the grid scale, FSS improvements for heavy rainfall reflect improved spatial placement, whereas SEEPS, which accounts for all rainfall categories, exhibits smaller yet consistent gains, indicating overall improvements in both the spatial distribution and categorical accuracy of precipitation forecasts. Together, these metrics show that Aeolus wind information mainly improves the representation of larger-scale features such as jetstreams and Rossby waves, which determine how cyclones and fronts, and thus rainfall systems develop and propagate.

In the Northern Hemisphere (NH), the impact is generally weaker than on the SH, but follows a similar seasonal pattern. One possible reason is that the NH jet tends to be less zonal and more dynamically variable, which may reduce the benefit from Aeolus wind observations, in addition to the already dense conventional observing network. During the extended boreal winter (December–February), when storm tracks are most active and the polar jet reaches peak strength, wind forecast error declines by about 1% in the troposphere during the first week of the forecast. These gains translate into small but consistent improvements in rainfall categories, with SEEPS rising to around 0.05% by day 10. FSS shows gains of about 2% for heavy rainfall thresholds above 10 mm/day at grid-scale after forecast day 7–8. As in the SH, this suggests that Aeolus contributes most strongly to the ability to predict the structure and movement of cyclones and frontal systems. During boreal summer, when storm tracks are weaker and large-scale wind–rain coupling is reduced, the benefits are smaller and more variable.

Aeolus has demonstrated remarkable benefits for NWP, remarkably so for a single satellite instrument with limited horizontal coverage, with the most pronounced downstream impacts during winter in both hemispheres, when jet dynamics govern storm development. These results confirm that better wind initial conditions translate into better predictions of jet dynamics and storm track evolution, which in turn improves heavy rainfall predictability. They also highlight the importance of sustaining and extending satellite wind lidar missions to further advance global weather forecasting.

Code availability. The analysis was conducted using the Python language and the code can be provided on request.

https://doi.org/10.5194/egusphere-2025-5219
Preprint. Discussion started: 11 November 2025

Data availability. The forecast data from the Observing System Experiment (OSE), were provided by the European Centre for Medium-Range Weather Forecasts (ECMWF). ERA5 reanalysis data are openly available from the Copernicus Climate Data Store (https://cds.climate.copernicus.eu). Precipitation observations from the Global Precipitation Measurement (GPM) mission, including the Integrated Multi-satellite Retrievals for GPM (IMERG) product, are freely accessible via NASA's Precipitation Measurement Missions (PMM) archive (https://pmm.nasa.gov/). More information and download instructions are available on the respective data portals.

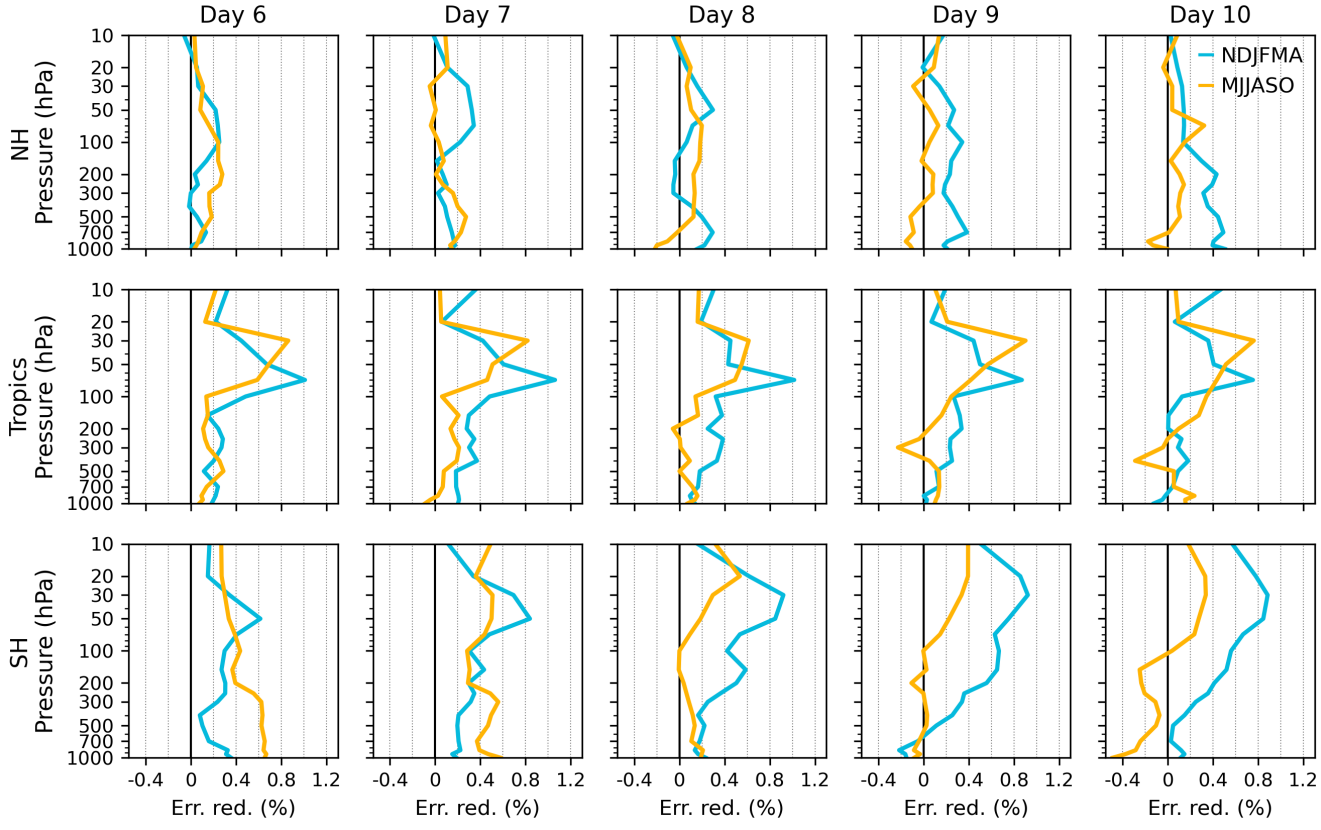

Figure A1. Same as Figure 4, but for forecast days 6 to 10.

Author contributions. MB, PK, and MW conceptualized the study and developed the methodology. MR performed the Observing System Experiments. PK provided funding acquisition and project supervision. MB was responsible for data curation, conducted the formal analysis, and wrote the original draft of the manuscript. All authors contributed to the interpretation of the results and reviewed and edited the manuscript.

https://doi.org/10.5194/egusphere-2025-5219
Preprint. Discussion started: 11 November 2025

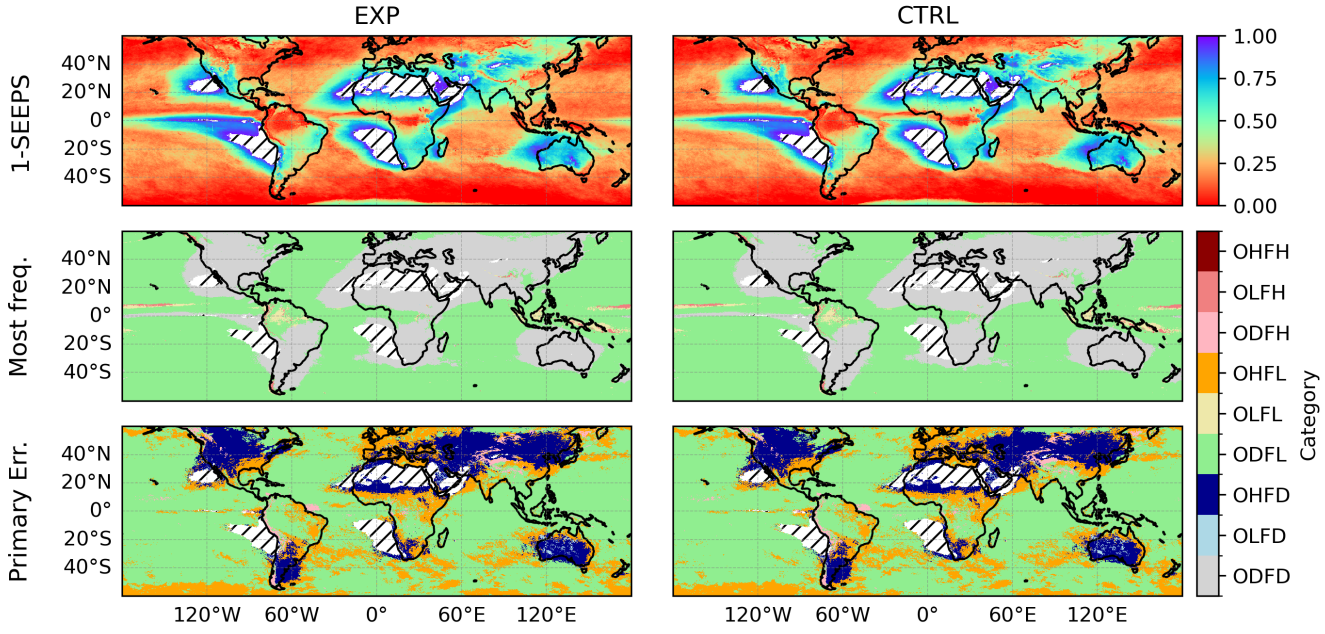

Figure A2. Day-3 precipitation forecast performance comparing the experiment with Aeolus wind assimilation (EXP, left column) to the control without Aeolus data (CTRL, right column). The top panels show the 1-SEEPS score, where values near 1 represent higher forecast. The middle panels illustrate the most frequently occurring observation–forecast category. The bottom panels identify the primary observation–forecast category that contributes most significantly to the SEEPS errors.

Competing interests. Some authors are members of the editorial board of Weather and Climate Dynamics.

Acknowledgements. We gratefully acknowledge the European Space Agency (ESA) for providing the Aeolus wind profile observations, and the European Centre for Medium-Range Weather Forecasts (ECMWF) for generating and sharing the observing system experiment (OSE) datasets. Their support and infrastructure made this research possible.

https://doi.org/10.5194/egusphere-2025-5219
Preprint. Discussion started: 11 November 2025

References

Baker, W. E., Atlas, R., Cardinali, C., Clement, A., Emmitt, G. D., Gentry, B. M., Hardesty, R. M., Källén, E., Kavaya, M. J., Langland, R., et al.: Lidar-measured wind profiles: The missing link in the global observing system, Bulletin of the American Meteorological Society, 95, 543–564, 2014.

Bauer, P., Geer, A. J., Lopez, P., and Salmond, D.: Direct 4D-Var assimilation of all-sky radiances. Part I: Implementation, Quarterly Journal of the Royal Meteorological Society, 136, 1868–1885, 2010.

Bechtold, P., Semane, N., Lopez, P., Chaboureau, J.-P., Beljaars, A., and Bormann, N.: Representing equilibrium and nonequilibrium convection in large-scale models, Journal of the Atmospheric Sciences, 71, 734–753, 2014.

Bonafoni, S., Biondi, R., Brenot, H., and Anthes, R.: Radio occultation and ground-based GNSS products for observing, understanding and predicting extreme events: A review, Atmospheric research, 230, 104 624, 2019.

Borne, M., Knippertz, P., Weissmann, M., Martin, A., Rennie, M., and Cress, A.: Impact of Aeolus wind lidar observations on the representation of the West African monsoon circulation in the ECMWF and DWD forecasting systems, Quarterly Journal of the Royal Meteorological Society, 149, 933–958, 2023.

Borne, M., Knippertz, P., Weissmann, M., Witschas, B., Flamant, C., Rios-Berrios, R., and Veals, P.: Validation of Aeolus L2B products over the tropical Atlantic using radiosondes, Atmospheric Measurement Techniques, 17, 561–581, 2024.

Bouttier, F. and Kelly, G.: Observing-system experiments in the ECMWF 4D-Var data assimilation system, Quarterly Journal of the Royal Meteorological Society, 127, 1469–1488, 2001.

Campbell, I. and Renwick, J. A.: Southern Hemisphere storm tracks and large-scale variability: What do the latest reanalyses say?, Journal of Climate, 36, 5549–5567, 2023.

Chou, C.-C. and Kushner, P. J.: Scale-dependent impact of Aeolus winds on a global forecast system, Quarterly Journal of the Royal Meteorological Society, 150, 373–387, 2024.

De Meutter, P., Gerard, L., Smet, G., Hamid, K., Hamdi, R., Degrauwe, D., and Termonia, P.: Predicting small-scale, short-lived downbursts: Case study with the NWP limited-area ALARO model for the Pukkelpop thunderstorm, Monthly Weather Review, 143, 742–756, 2015.

Derin, Y. and Yilmaz, K. K.: Evaluation of multiple satellite-based precipitation products over complex topography, Journal of Hydrometeorology, 15, 1498–1516, 2014.

Derin, Y., Anagnostou, E., Berne, A., Borga, M., Boudevillain, B., Buytaert, W., Chang, C.-H., Chen, H., Delrieu, G., Hsu, Y. C., et al.: Evaluation of GPM-era global satellite precipitation products over multiple complex terrain regions, Remote Sensing, 11, 2936, 2019.

Dinku, T., Connor, S. J., and Ceccato, P.: Comparison of CMORPH and TRMM-3B42 over mountainous regions of Africa and South America, Satellite rainfall applications for surface hydrology, pp. 193–204, 2010.

Dong, B., Sutton, R. T., Woollings, T., and Hodges, K.: Variability of the North Atlantic summer storm track: mechanisms and impacts on European climate, Environmental Research Letters, 8, 034 037, 2013.

Ebert, E. E.: Fuzzy verification of high-resolution gridded forecasts: a review and proposed framework, Meteorological Applications: A journal of forecasting, practical applications, training techniques and modelling, 15, 51–64, 2008.

Feng, Z., Leung, L. R., Hagos, S., Houze, R. A., Burleyson, C. D., and Balaguru, K.: More frequent intense and long-lived storms dominate the springtime trend in central US rainfall, Nature communications, 7, 13 429, 2016.

Forbes, R., Haiden, T., and Magnusson, L.: Improvements in IFS forecasts of heavy precipitation, ECMWF Newsletter, 144, 21–26, 2015.

Gandin, L. S. and Murphy, A. H.: Equitable skill scores for categorical forecasts, Monthly weather review, 120, 361–370, 1992.

https://doi.org/10.5194/egusphere-2025-5219
Preprint. Discussion started: 11 November 2025

Geer, A. J., Bauer, P., and Lopez, P.: Direct 4D-Var assimilation of all-sky radiances. Part II: Assessment, Quarterly Journal of the Royal Meteorological Society, 136, 1886–1905, 2010.

Gilleland, E., Ahijevych, D., Brown, B. G., Casati, B., and Ebert, E. E.: Intercomparison of spatial forecast verification methods, Weather and forecasting, 24, 1416–1430, 2009.

Hersbach, H., Bell, B., Berrisford, P., Hirahara, S., Horányi, A., Muñoz-Sabater, J., Nicolas, J., Peubey, C., Radu, R., Schepers, D., et al.: The ERA5 global reanalysis, Quarterly Journal of the Royal Meteorological Society, 146, 1999–2049, 2020.

Hirpa, F. A., Gebremichael, M., and Hopson, T.: Evaluation of high-resolution satellite precipitation products over very complex terrain in Ethiopia, Journal of Applied Meteorology and Climatology, 49, 1044–1051, 2010.

Hobouchian, M. P., Salio, P., Skabar, Y. G., Vila, D., and Garreaud, R.: Assessment of satellite precipitation estimates over the slopes of the subtropical Andes, Atmospheric Research, 190, 43–54, 2017.

Huffman, G. J., Bolvin, D. T., Braithwaite, D., Hsu, K., Joyce, R., Xie, P., and Yoo, S.-H.: NASA global precipitation measurement (GPM) integrated multi-satellite retrievals for GPM (IMERG), Algorithm Theoretical Basis Document (ATBD) Version, 4, 26, 2015.

Kelly, G., McNally, T., Thépaut, J., and Szyndel, M.: OSEs of all main data types in the ECMWF operation system, in: Proc. Third WMO Workshop on the Impact of Various Observing Systems on Numerical Weather Prediction, pp. 63–94, 2004.

Lux, O., Rennie, M., de Kloe, J., and Reitebuch, O.: Five years of Aeolus wind profiling: global coverage and data quality, EGUsphere, 2025, 1–46, 2025.

Ma, C.-G. and Chang, E. K.: Impacts of storm-track variations on wintertime extreme weather events over the continental United States, Journal of Climate, 30, 4601–4624, 2017.

Marseille, G. and Stoffelen, A.: Simulation of wind profiles from a space-borne Doppler wind lidar, Quarterly Journal of the Royal Meteorological Society: A journal of the atmospheric sciences, applied meteorology and physical oceanography, 129, 3079–3098, 2003.

Martin, A., Weissmann, M., and Cress, A.: Impact of assimilating Aeolus observations in the global model ICON: A global statistical overview, Quarterly Journal of the Royal Meteorological Society, 149, 2962–2979, 2023a.

Martin, A., Weissmann, M., and Cress, A.: Investigation of links between dynamical scenarios and particularly high impact of Aeolus on numerical weather prediction (NWP) forecasts, Weather and Climate Dynamics, 4, 249–264, 2023b.

Matsuno, T.: Quasi-geostrophic motions in the equatorial area, Journal of the Meteorological Society of Japan. Ser. II, 44, 25–43, 1966.

Murphy, A. H. and Winkler, R. L.: A general framework for forecast verification, Monthly weather review, 115, 1330–1338, 1987.

Prakash, S., Mitra, A. K., Pai, D., and AghaKouchak, A.: From TRMM to GPM: How well can heavy rainfall be detected from space?, Advances in Water Resources, 88, 1–7, 2016.

Prein, A. F., Langhans, W., Fosser, G., Ferrone, A., Ban, N., Goergen, K., Keller, M., Tölle, M., Gutjahr, O., Feser, F., et al.: A review on regional convection-permitting climate modeling: Demonstrations, prospects, and challenges, Reviews of geophysics, 53, 323–361, 2015.

Reitebuch, O.: The spaceborne wind lidar mission ADM-Aeolus, in: Atmospheric physics: Background–methods–trends, pp. 815–827, Springer, 2012.

Rennie, M. and Isaksen, L.: The NWP impact of Aeolus Level-2B winds at ECMWF, https://doi.org/10.21957/d4ea1c09d4, 2024.

Rennie, M., Healy, S., Abdalla, S., McLean, W., and Henry, K.: Aeolus positive impact on forecasts with the second reprocessed dataset, ECMWF newsletter, 173, 14–20, 2022.

Rennie, M. P., Isaksen, L., Weiler, F., de Kloe, J., Kanitz, T., and Reitebuch, O.: The impact of Aeolus wind retrievals on ECMWF global weather forecasts, Quarterly Journal of the Royal Meteorological Society, 147, 3555–3586, 2021.

https://doi.org/10.5194/egusphere-2025-5219
Preprint. Discussion started: 11 November 2025

Roberts, N.: Assessing the spatial and temporal variation in the skill of precipitation forecasts from an NWP model, Meteorological Applications: A journal of forecasting, practical applications, training techniques and modelling, 15, 163–169, 2008.

Rodwell, M. J., Richardson, D. S., Hewson, T. D., and Haiden, T.: A new equitable score suitable for verifying precipitation in numerical weather prediction, Quarterly Journal of the Royal Meteorological Society, 136, 1344–1363, 2010.

Stoffelen, A., Pailleux, J., Källén, E., Vaughan, J. M., Isaksen, L., Flamant, P., Wergen, W., Andersson, E., Schyberg, H., Culoma, A., et al.: The atmospheric dynamics mission for global wind field measurement, Bulletin of the American Meteorological Society, 86, 73–88, 2005.

Stoffelen, A., Marseille, G.-J., Bouttier, F., Vasiljevic, D., De Haan, S., and Cardinali, C.: ADM-Aeolus Doppler wind lidar observing system simulation experiment, Quarterly Journal of the Royal Meteorological Society: A journal of the atmospheric sciences, applied meteorology and physical oceanography, 132, 1927–1947, 2006.

Straume, A.-G., Rennie, M., Isaksen, L., de Kloe, J., Marseille, G.-J., Stoffelen, A., Flament, T., Stieglitz, H., Dabas, A., Huber, D., et al.: ESA's space-based Doppler wind lidar mission Aeolus–First wind and aerosol product assessment results, in: EPJ Web of Conferences, vol. 237, p. 01007, EDP Sciences, 2020.

Taylor, C. M., Belušić, D., Guichard, F., Parker, D. J., Vischel, T., Bock, O., Harris, P. P., Janicot, S., Klein, C., and Panthou, G.: Frequency of extreme Sahelian storms tripled since 1982 in satellite observations, Nature, 544, 475–478, 2017.

Thiemig, V., Rojas, R., Zambrano-Bigiarini, M., Levizzani, V., and De Roo, A.: Validation of satellite-based precipitation products over sparsely gauged African river basins, Journal of Hydrometeorology, 13, 1760–1783, 2012.

Walz, E.-M., Maranan, M., van der Linden, R., Fink, A. H., and Knippertz, P.: An IMERG-based optimal extended probabilistic climatology (EPC) as a benchmark ensemble forecast for precipitation in the tropics and subtropics, Weather and Forecasting, 36, 1561–1573, 2021.

Weissmann, M. and Cardinali, C.: Impact of airborne Doppler lidar observations on ECMWF forecasts, Quarterly Journal of the Royal Meteorological Society: A journal of the atmospheric sciences, applied meteorology and physical oceanography, 133, 107–116, 2007.

Weissmann, M., Langland, R. H., Cardinali, C., Pauley, P. M., and Rahm, S.: Influence of airborne Doppler wind lidar profiles near Typhoon Sinlaku on ECMWF and NOGAPS forecasts, Quarterly Journal of the Royal Meteorological Society, 138, 118–130, https://doi.org/https://doi.org/10.1002/qj.896, 2012.

Wheeler, M. and Kiladis, G. N.: Convectively coupled equatorial waves: Analysis of clouds and temperature in the wavenumber–frequency domain, Journal of the Atmospheric Sciences, 56, 374–399, 1999.

Yang, G.-Y. and Slingo, J.: The diurnal cycle in the tropics, Monthly Weather Review, 129, 784–801, 2001.

Žagar, N.: Assimilation of equatorial waves by line-of-sight wind observations, Journal of the atmospheric sciences, 61, 1877–1893, 2004.

Žagar, N., Stoffelen, A., Marseille, G.-J., Accadia, C., and Schlüssel, P.: Impact assessment of simulated Doppler wind lidars with a multivariate variational assimilation in the tropics, Monthly weather review, 136, 2443–2460, 2008.

Žagar, N., Pilch Kedzierski, R., De Chiara, G., Healy, S., Rennie, M., and Sielmann, F.: ESA's Aeolus mission reveals uncertainties in tropical wind and wave-driven circulations, Geophysical Research Letters, 52, e2025GL114 832, 2025.